DOI: 10.26599/FSHW.2026.9251121

Contents lists available at SciOpen

Food Science and Human Wellness

journal homepage: https://www.sciopen.com/journal/2097-0765

China Food Publishing Co.

Rosmarinic acid, the key dietary antioxidant in *Rosmarinus officinalis* L. identified by integrated screening, targets PPARγ to activate Nrf2/NQO1 axis and mitigate oxidative stress

Zhenhua Liang[a,b#], Haiyang Liang[a#], Wenfeng Shi[a#], Dongqi Liu[a], Yinfei Sun[a], Zhenhua Liu[a,b,c,d*], Wenyi Kang[a,b,c,d*]

[a] *National R & D Center for Edible Fungus Processing Technology, Henan University, Kaifeng 475004, China*

[b] *College of Agriculture, Henan University, Kaifeng 475004, China*

[c] *Joint International Research Laboratory of Food & Medicine Resource Function, Henan Province, Kaifeng 475004, China*

ABSTRACT: Although *Rosmarinus officinalis* L. (rosemary) is widely consumed as a prominent source of natural antioxidants, its specific bioactive constituents and precise molecular targets against oxidative stress remain elusive. This study aimed to identify the core functional ingredients of rosemary and elucidate their underlying protective mechanisms. Through an integrated screening strategy combining untargeted metabolomics, spectrum-effect analysis, and a component knock-out method, rosmarinic acid (RA) was identified as the pivotal dietary antioxidant. The efficacy of RA was validated in hydrogen peroxide (H_2O_2)-challenged HepG2 cells and 2,2'-azobis(2-amidinopropane) dihydrochloride (AAPH)-challenged zebrafish models, where RA effectively mitigated oxidative damage by suppressing reactive oxygen species (ROS) accumulation and apoptosis. Mechanistically, RA upregulated peroxisome proliferator-activated receptor gamma (PPARγ) expression and activated downstream nuclear factor erythroid 2-related factor 2 (Nrf2)/NAD(P)H quinone dehydrogenase 1 (NQO1) pathway. Concurrently, RA attenuated MAPK1 and STAT1 phosphorylation and inhibited cleaved-Caspase-3 activation. Crucially, molecular docking (binding affinity: -9.038 kcal/mol) and Cellular Thermal Shift Assay (CETSA) confirmed the direct physical binding of RA to PPARγ. In conclusion, RA is the core bioactive compound in rosemary that exerts potent cytoprotective effects by directly targeting PPARγ to activate the antioxidant Nrf2/NQO1 axis. These findings provide a robust scientific basis for utilizing rosemary and RA as functional food ingredients to combat oxidative stress-related pathologies.

Keywords: *Rosmarinus officinalis* L., Functional food, Oxidative stress, Rosmarinic acid, Spectrum-effect relationship, PPARγ, Nrf2-NQO1 pathway, Dietary antioxidant

1. Introduction

Excessive accumulation of reactive oxygen species (ROS) drives oxidative stress, a pathological state that precipitates cellular dysfunction and contributes to aging and a spectrum of chronic metabolic and neurodegenerative disorders[1-3]. Particularly in the liver, the body's primary metabolic and detoxifying organ, oxidative stress acts as a critical driver in the onset and progression of various hepatic pathologies,

# These authors contributed equally to this work.
*** Corresponding author.**
Zhenhua Liu, E-mail: liuzhenhua623@163.com;
Wenyi Kang, E-mail: kangweny@hotmail.com

Received 27 February 2026
Received in revised from 22 April 2026
Accepted 11 May 2026

ranging from non-alcoholic fatty liver disease (NAFLD) to drug-induced liver injury and hepatocellular carcinoma[4, 5]. Consequently, mitigating hepatic oxidative damage has emerged as a crucial strategy for the prevention of liver-related diseases. In the physiological defense against such environmental and metabolic insults, the transcription factor nuclear factor erythroid 2-related factor 2 (Nrf2) plays an indispensable role in maintaining cellular redox homeostasis. Crucially, the protective capacity of Nrf2 is intricately regulated by upstream signaling cascades, wherein peroxisome proliferator-activated receptor gamma (PPARγ) acts as a critical node. Emerging evidence indicates a synergistic interplay between PPARγ and Nrf2; PPARγ activation upregulates Nrf2 expression and facilitates its nuclear translocation, thereby forming a robust PPARγ-Nrf2 defense axis against cellular oxidative injury[6, 7]. Given the prevalence of adverse effects associated with synthetic antioxidants, there is a growing global interest in utilizing safe and effective natural antioxidants derived from daily diets and edible plants to mitigate oxidative stress[8, 9]. Consequently, identifying key dietary antioxidant constituents from these dual-purpose botanical resources to develop functional foods has become a primary research focus in food science and nutrition.

Rosmarinus officinalis L. (rosemary) is a widely consumed culinary herb and a prominent source of natural antioxidants[10]. Extensive research has documented its diverse array of bioactive compounds, including rosmarinic acid, carnosic acid, and various flavonoids and phenolic acids, which can efficiently neutralize free radicals and mitigate cellular damage[11]. Beyond its fundamental antioxidant capacity, rosemary serves a dual role as a natural preservative in the food industry and a health-promoting dietary agent for preventing chronic diseases[12]. Specifically, accumulating evidence highlights the potent pharmacological efficacy of rosemary extracts and their primary constituent, rosmarinic acid (RA), particularly with particular emphasis on their hepatoprotective, anti-inflammatory, and anti-apoptotic properties. Recent studies have demonstrated that RA can effectively alleviate hepatic oxidative injury, lipid peroxidation, and cellular apoptosis in various experimental models[13, 14]. However, despite its widespread application as a food ingredient, the specific phytochemical basis responsible for its health benefits remains elusive due to the chemical complexity of its extracts. Furthermore, existing mechanistic studies have predominantly relied on phenotypic observations, lacking robust evidence regarding the direct target engagement between specific dietary components and their exact molecular targets.

To bridge these knowledge gaps, this study aimed to identify the core functional antioxidant ingredients in rosemary and elucidate their precise molecular targets for dietary intervention. Unlike previous research that predominantly focused on the general efficacy of crude extracts or lacked direct target validation, this study is distinguished by its multidimensional and targeted methodology. We designed an integrated food-chemistry screening strategy combining untargeted metabolomics, spectrum-effect relationship analysis, and a novel "component knock-out" method to systematically isolate the pivotal dietary bioactive compounds. Subsequently, we sought to evaluate the protective efficacy and investigate the underlying molecular mechanisms-specifically targeting the peroxisome proliferator-activated receptor gamma (PPARγ) and the Nrf2 pathway-using in vitro HepG2 cells and in vivo zebrafish models. Furthermore, a

major innovative aspect of our work is the transition from purely phenotypic observations to the confirmation of direct target engagement. By utilizing the Cellular Thermal Shift Assay (CETSA) and molecular docking, this study provides compelling empirical evidence of direct physical binding between the active constituent and PPARγ. Through this comprehensive approach, the objective of this work is to provide a robust scientific foundation for the application of rosemary and its core active constituents as functional food ingredients to promote human metabolic and cellular health.

2. Materials and methods

2.1 Reagents and Plant Materials

Fresh leaves of *Rosmarinus officinalis* L. (Rosemary) were collected from 15 distinct regions across Henan Province, China, in April 2023. The botanical identification was authenticated by Professor Changqin Li from the National R & D Center for Edible Fungus Processing Technology. All samples were air-dried to a constant weight and stored as intact leaves in sealed bags, and voucher specimens have been deposited at the Herbarium of the National Edible Fungi Processing Technology R&D Center. RA standard (purity>98%) used for cell and animal experiments was purchased from Sigma-Aldrich. 2,2′-Azino-bis(3-ethylbenzothiazoline-6-sulfonic acid) (ABTS) was purchased from Fluka (St. Louis, MO, USA). HPLC-grade formic acid (FA, 98%), acetonitrile (ACN, ≥99.9%), and ethanol (≥99.9%) were procured from Thermo Fisher Scientific (Waltham, MA, USA).

2.2 Preparation of Rosemary Ethanol Extract (RO-EE)

Take 30 g of rosemary leaves and add 15 times the volume of 75% ethanol (w/v). Soak the mixture three times, with extraction durations of 48 h, 48 h, and 24 h, respectively. Filter the mixture, combine the filtrates, and concentrate under reduced pressure until a viscous consistency is achieved. Freeze-dry the mixture to obtain a solid powder (7.727 g), yielding a yield of approximately 25.76%[15, 16].

2.3 Non-targeted metabolomics and network pharmacology

2.3.1 Metabolite extraction

Weigh 50 mg of sample and place it in a 1°C water bath for ultrasonication for 30 minutes. Then, allow it to stand at -20°C for 1 hour. Centrifuge at 4°C and 14,000 rpm for 15 minutes. After centrifugation, take 600 μL of the supernatant, filter it through a 0.22 μm membrane, and place the filtered sample in a sample vial for LC-MS analysis. Take 20 μL from each sample and combine them to form a QC control sample, used to evaluate the repeatability and stability of the LC-MS analytical process.

2.3.2 Non-targeted metabolomics analysis (LC-MS/MS)

Metabolite separation and detection were performed using a Waters ACQUITY™ 2D UPLC system (Waters, Milford, MA, USA) coupled with a Q Exactive™ high-resolution mass spectrometer (Thermo Fisher Scientific, Waltham, MA, USA). The untargeted metabolomics analysis and data processing were conducted by BGI-Shenzhen (Shenzhen, China).

2.3.3 Screening of active components and target prediction

Potential active ingredients of Rosmarinus officinalis were initially screened using the Traditional Chinese Medicine Systems Pharmacology Database and Analysis Platform (TCMSP) [17]and the SwissADME database (http://www.swissadme.ch/). The screening criteria in TCMSP were set as oral bioavailability (OB) ≥ 30% and drug-likeness (DL) ≥ 0.18. In SwissADME, candidate compounds were required to meet the following conditions: (1) high gastrointestinal (GI) absorption; and (2) compliance with at least three of the five drug-likeness rules (Lipinski, Ghose, Veber, Egan, and Muegge). Compounds satisfying both TCMSP and SwissADME criteria were selected for further analysis. Subsequently, the putative targets of these active ingredients were retrieved from the TCMSP database (https://tcmspw.com/tcmsp.php) and predicted using the SwissTargetPrediction web server, with a probability threshold of > 0.1. All target protein names were standardized using the UniProt database (https://www.uniprot.org/).

2.3.4 Acquisition of oxidative stress-related targets

To identify disease-associated targets, the keyword "Oxidative" was used to query multiple databases, including GeneCards (https://www.genecards.org/), OMIM (https://omim.org/), TTD (http://db.idrblab.net/ttd/), PharmGKB (https://www.pharmgkb.org/), and DrugBank (https://go.drugbank.com/). The intersection of results from these databases was compiled as the dataset of oxidative stress-related targets.

2.3.5 Construction and analysis of the PPI network

The intersection between the targets of active components and the oxidative stress-related targets was identified as the potential therapeutic targets of RO-EE against oxidative stress. These overlapping targets were imported into the STRING database (https://www.string-db.org/) to construct a protein-protein interaction (PPI) network[18]. Topological analysis was then performed based on the interaction data.

2.3.6 Molecular docking

Crystal structures of targets (PPARG, CASP3, MAPK1, STAT1) and the ligand (RA) were retrieved from the PDB and PubChem databases, respectively. Molecular docking was performed using AutoDock Vina, and interactions were visualized using PyMOL and Discovery Studio[19-21].

2.4 Spectrum-effect relationship and component knock-out

2.4.1 HPLC fingerprinting conditions

Chromatographic separation utilized an RP-18 endcapped column (4.6 × 250 mm, 5 μm) maintained at 30°C with detection at 280 nm. The mobile phase (0.8 mL/min) consisted of acetonitrile (A) and 0.1% aqueous formic acid (B) with the following gradient: 0-30 min, 10%-20% A; 30-70 min, 20%-30% A; 70-110 min, 30%-40% A; and 110-210 min, 40%-50% A.

2.4.2 Partial Least Squares (PLS) analysis

Fingerprint data were standardized using the Similarity Evaluation System for Chromatographic Fingerprint of TCM (2012 Edition). Partial Least Squares Regression (PLSR) was performed via DPS 7.05 software, correlating peak areas (X) with ABTS scavenging rates (Y) to identify bioactive peaks.

2.4.3 Preparation of knock-out components

Using the HPLC protocol above, fractions containing target peaks (high resolution/abundance) and the remaining eluate were separately collected, concentrated, and filtered (0.22 μm). These were designated as the target-containing sample (Px+) and negative control (Px-), respectively.

2.4.4 LC-MS/MS identification

LC separation was performed on a Waters XBridge BEH C_{18} column (2.1 × 100 mm, 2.5 μm) using 5 mM aqueous ammonium formate (A) and acetonitrile (B) at 0.25 mL/min. The gradient was: 0-1 min, 5% B; 1-12 min, 5%-95% B; 12-17 min, 95% B; and 17.1-20 min, 5% B. Mass spectrometry employed an ESI source (positive/negative modes) with the following parameters: spray voltage, 5500 V; source temperature, 400°C; curtain gas, 0.24 MPa; nebulizer/auxiliary gas, 0.34/0.38 MPa. TOF-MS (50-1000 Da) used a 0.15 s accumulation time and 80 V declustering potential. IDA-MS/MS operated in high sensitivity mode (0.05 s accumulation) with a collision energy of 35 ± 15 eV and dynamic isotope exclusion.

2.5 Evaluation of antioxidant activity

The ABTS radical scavenging capacity was determined as previously described[22]. Briefly, samples were incubated with $ABTS^+$ working solution for 30 min, and absorbance was measured at 405 nm. The scavenging rate was calculated as follows:

$$ABTS\ radical\ scavenging\ rate\ (\%) = [1 - (A\ sample - A\ control) \div A\ control] \times 100\%$$

where A_{sample} and $A_{control}$ denote the absorbance of the sample and control, respectively.

2.6 In vitro experiments

2.6.1 Cell culture

HepG2 cells were maintained in high-glucose DMEM supplemented with 10% fetal bovine serum (FBS) and 1% penicillin-streptomycin at 37°C in a humidified 5% CO_2 atmosphere. After reaching the logarithmic growth phase, the HepG2 cells were treated with rosmarinic acid, carnosic acid, carnosol, or cirsimaritin at gradient concentrations (12.5–200.0 μM) for 24 h.

2.6.2 Cell viability assay

Cell viability was determined using the MTT assay following our previously described method[23]. Briefly, HepG2 cells were treated with rosmarinic acid, carnosic acid, carnosol, or cirsimaritin at gradient concentrations (12.5–200.0 μM) for 24 h. The absorbance was measured at 490 nm (reference: 630 nm).

2.6.3 Measurement of intracellular ROS

Intracellular ROS levels were quantified using the DCFH-DA probe via flow cytometry, strictly according to the protocol detailed in our previous study[23]. Cells in the logarithmic growth phase were uniformly inoculated into the 6-well cell culture plate, and the experimental groups were set as described in Section 2.6.1. After cultivation in the incubator for 24 h, the cells were collected. ROS fluorescent probes were then added to the cell culture plate. Then, the culture plate was incubated on ice in the dark for 30 min. After washing the cells three times with PBS solution, the cells were harvested via filtration using a 300-mesh nylon membrane, and examined immediately by flow cytometry. For each sample, 10^4 cells were detected, and the results were analyzed by the CytExpert software.

2.6.4 Assessment of oxidative stress markers

After treatment, protein concentration was determined using a BCA kit (Solarbio). The levels of MDA and activities of SOD, CAT, and GSH in cell lysates were measured using commercial kits (Nanjing Jiancheng Bioengineering Institute, China) following the manufacturer's protocols.

2.6.5 Cellular Thermal Shift Assay (CETSA)

The CETSA procedure followed the experimental protocol published in the literature[24, 25]. HepG2 cell lysates were prepared by five cycles of rapid freeze-thaw in liquid nitrogen. Lysates were incubated with or without cornuside for 2 h, then heated individually at graded temperatures (50-59°C) for 3 min. After heating, samples were immediately cooled on ice. Soluble fractions were separated by centrifugation and analyzed for CDK2 levels by Western blotting.

2.7 In vivo zebrafish experiments

2.7.1 Zebrafish maintenance and drug treatment

Zebrafish (wild-type AB) maintenance and embryo collection were strictly conducted according to our previous protocol[26]. Crucially, all animal care and experimental procedures specific to this study were officially approved by the Institutional Animal Care and Use Committee (IACUC) of Animal Experiment Center of Henan University. Healthy larvae at 3 days post-fertilization (dpf) were randomly divided into six groups (n = 30): Control, Model (12.5 mM AAPH), Positive (Vitamin C, 50 μM), and treatment groups (Low, Medium, High). Drug administration was performed via co-treatment with AAPH for 18 h as previously described.

2.7.2. Determination of ROS and cell death

The levels of intracellular ROS and cell death were evaluated using DCFH-DA and Acridine Orange (AO) staining, respectively. The staining procedures, image acquisition, and fluorescence quantification using ImageJ software were performed following the detailed methods described in our previous study[26].

2.8 Quantitative Real-Time PCR (qRT-PCR)

Quantitative real-time PCR was performed as previously described with minor modifications[27]. Quantitative PCR was performed on a Quant Studio 3 system (Applied Biosystems, USA) to determine mRNA expression levels of *PPARG*、*DPP4*、*PRSS1*、*MAPK1*、*Caspase 3*、*STAT1*、*CDKN1A*、

PTGS2、*ESR1*、*ERK*、*STAT1b*、*nrf2*、*nqo1*、*cat*、*sod*、*gpx1*, using β-actin as the internal control. The primer sequences used in this study are listed in Table S1.

2.9 Western Blot

The Western blot procedure followed a previously published protocol from our laboratory[28, 29]. Total protein was extracted from cells using RIPA lysis buffer and quantified with a bicinchoninic acid (BCA) assay kit (Solarbio, China). Proteins were separated by SDS-PAGE, transferred to PVDF membranes, blocked with 5% non-fat milk, and incubated with primary antibodies followed by horseradish peroxidase (HRP)-conjugated secondary antibodies. Protein bands were detected using an enhanced chemiluminescence (ECL) kit and visualized with a chemiluminescence imaging system. Band intensities were quantified by densitometry, normalized to β-actin as loading control, and expressed relative to the control group.

2.10 Statistical Analysis

Statistical analysis was performed using GraphPad Prism 8.0 (GraphPad Software, San Diego, CA, USA). Data are expressed as mean ± standard deviation (SD). Prior to assessing statistical significance, the data were tested for normality using the Shapiro-Wilk test and for homogeneity of variances using Levene's test. For data meeting these assumptions, multiple group comparisons were analyzed using one-way analysis of variance (ANOVA) followed by Tukey's post-hoc test. If the assumptions of normal distribution or homogeneity of variances were not met, the non-parametric Kruskal-Wallis test followed by Dunn's multiple comparisons test was employed. A P-value < 0.05 was considered statistically significant. Significance levels are denoted as follows: */# $P < 0.05$, **/## $P < 0.01$, ***/### $P < 0.001$, and ****/#### $P < 0.0001$.

3. Results

3.1 Identification of bioactive components and prediction of therapeutic targets based on untargeted metabolomics and network pharmacology

To elucidate the key antioxidant constituents of rosemary and their corresponding molecular targets, we first conducted an untargeted metabolomics analysis. Using strict identification criteria (Match score > 85 and identification level > 2), a total of 266 chemical components were identified from RO-EE, including 157 in positive ion mode and 109 in negative ion mode. Based on the screening criteria described in Section 2.3.3, 45 high-quality active ingredients were filtered out, which were predicted to target 379 unique proteins (Fig. 1A). As detailed in Table S2, these bioactive compounds were predominantly classified as fatty acyls and terpenoids.

Subsequently, to map the therapeutic mechanism, 7,884 targets related to oxidative stress were retrieved from five public databases (GeneCards, OMIM, PharmGKB, TTD, and DrugBank) after removing duplicates (Fig. 1B). The intersection of drug targets and disease targets yielded 338 common targets, which were regarded as the potential therapeutic targets of RO-EE against oxidative stress (Fig. 1C). These overlapping targets and the active components were imported into Cytoscape 3.8.0 to construct a

"Component-Target" regulatory network (Fig. 1D). Topological analysis identified 23 main targets with a Degree value ≥ 5 (Fig. 1E). The number of compounds corresponding to these proteins indicates that targets interacting with multiple active ingredients are likely the primary drivers of the antioxidant effects.

To further narrow down the core mediators, the overlapping targets were mapped into the STRING database to construct a protein-protein interaction (PPI) network. Based on topological analysis, targets meeting the criteria of "BC, CC, EC, LAC, and NC > median" and "DC > 2 × median" were selected as key hubs. Consequently, 22 core targets were identified, including HSP90AB1, STAT1, HSP90AA1, CDK1, ESR1, CASP3, PTK2, IL6, ERBB2, TP53, CDK2, STAT3, CDKN1A, EP300, BCL2, MDM2, CDK4, CCND1, BCL2L1, MAPK1, EGFR, and AKT1 (Fig. 1F). Further analysis of the number of compounds corresponding to targets within this core network (Fig. 1G) indicates that multi-compound targeting is the core mechanism underlying rosemary's antioxidant activity.

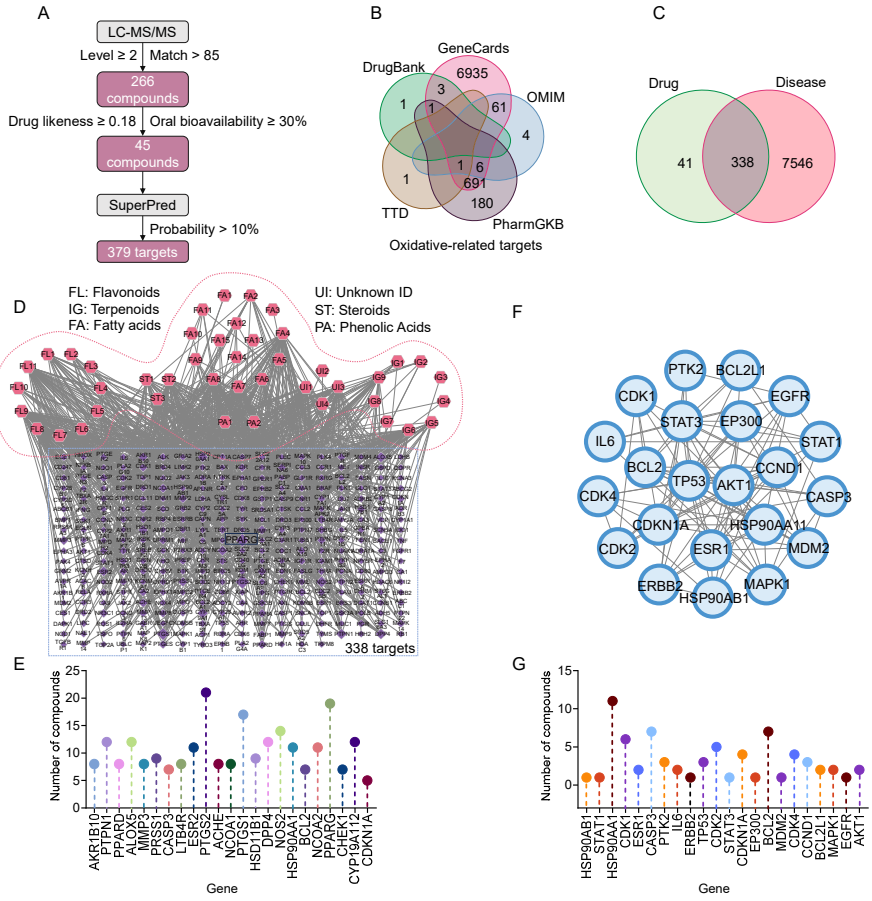

Fig. 1. Screening of bioactive ingredients and prediction of therapeutic targets using metabolomics and network pharmacology. (A) Target Screening Workflow. (B) Venn diagram of targets related to oxidative stress retrieved from public databases. (C) Venn diagram showing the intersection between Rosmarinus officinalis L. extract (RO-EE) potential targets and oxidative stress-related targets. (D) The "Component-Target" network of RO-EE. (E) Analysis of compound numbers targeting major targets based on degree values ≥5. (F) Protein-Protein Interaction (PPI) network of core targets constructed via the STRING database. (G) Analysis of compound numbers acting on core network nodes.

3.2 Screening of antioxidant material basis via spectrum-effect relationship analysis and HPLC "knock-out" strategy

To profile the phytochemical landscape and evaluate the compositional consistency of dietary rosemary extracts, HPLC fingerprints of 15 batches were established, revealing 17 common peaks (P1–P17) (Fig. 2A).

Chemometric analyses, including Hierarchical Cluster Analysis (HCA) and Principal Component Analysis (PCA), classified these batches into four distinct clusters based on peak areas (Fig. S1A, B), indicating intrinsic quantitative variations in the chemical composition among the samples. In the ABTS radical scavenging assay, batch S10 exhibited the most potent antioxidant capacity (lowest IC50 value) and was thus selected as the representative matrix for in-depth food-chemistry analysis (Fig. 2B, C). To decipher the material basis responsible for this efficacy, a Partial Least Squares-Discriminant Analysis (PLS-DA) model was constructed to correlate the chromatographic peaks with the antioxidant phenotypes. As depicted in Fig. 2D, peaks P3, P4, P5, P6, P9, P10, P12, P15, and P17 exhibited a strong positive correlation (R > 0.1) with the ABTS scavenging capacity, highlighting their potential roles as the primary functional contributors.

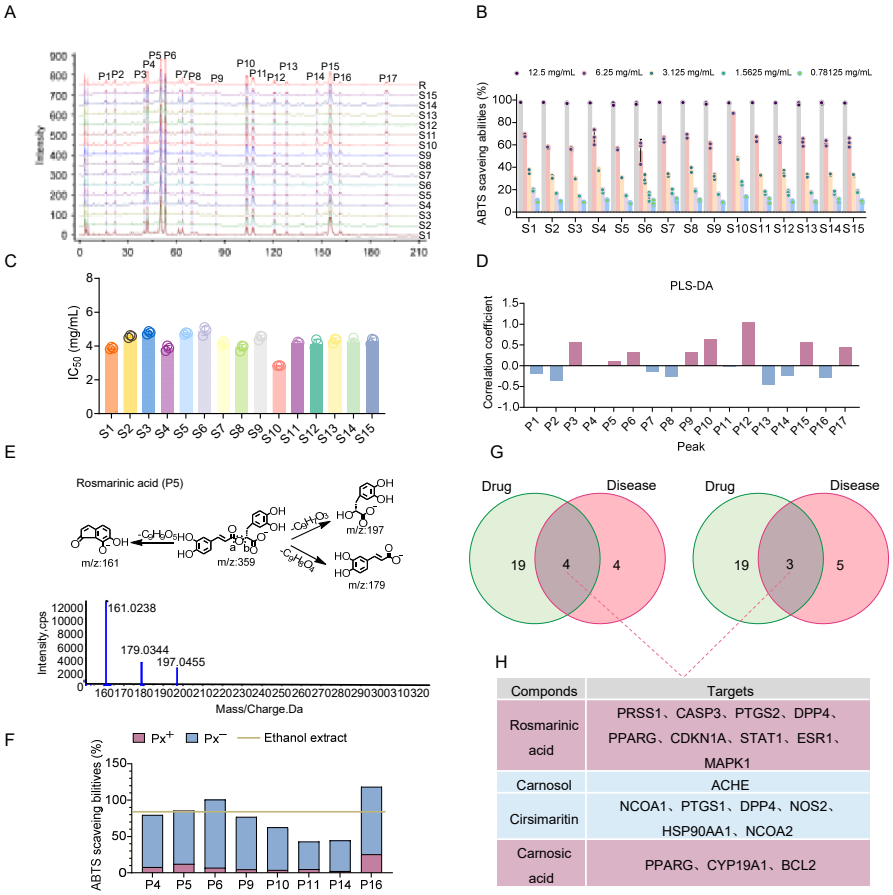

Componds	Targets
Rosmarinic acid	PRSS1、CASP3、PTGS2、DPP4、PPARG、CDKN1A、STAT1、ESR1、MAPK1
Carnosol	ACHE
Cirsimaritin	NCOA1、PTGS1、DPP4、NOS2、HSP90AA1、NCOA2
Carnosic acid	PPARG、CYP19A1、BCL2

Fig. 2. Identification of core dietary antioxidants in *Rosmarinus officinalis* L. utilizing an integrated spectrum-effect relationship and component knock-out strategy. (A) Representative HPLC chromatograms of 15 batches of rosemary extracts and the generated reference fingerprint (R). (B) Evaluation of ABTS radical scavenging capacity across the 15 batches of rosemary samples. (C) Calculated IC_{50} values representing the varied antioxidant efficacy of the 15 batches. (D) Partial Least Squares Regression (PLSR) analysis illustrating the correlation between common chromatographic peaks and ABTS radical scavenging activity. (E) Representative MS/MS fragmentation spectrum for the structural elucidation of rosmarinic acid (RA). (F) Comparison of ABTS scavenging rates among the original extract, specific component knock-out fractions, and negative controls to validate individual functional contributions. (G) Venn diagram detailing the intersection between the analytically validated knock-out compounds and the bioactive candidates predicted via network pharmacology. (H) Final prioritization of the key dietary bioactive constituents and their corresponding molecular targets.

To definitively identify these functional constituents and validate their exact contributions, a novel "component knock-out" strategy was applied to sequentially isolate the high-resolution peaks (R > 1.5). By cross-referencing MS/MS fragmentation patterns with existing analytical databases, the knock-out peaks were structurally elucidated as oxolinic acid (P4), rosmarinic acid (P5), carnosic acid (P6), morusin (P9),

cirsimaritin (P10), isorhamnetin (P11), carnosol (P14), and cortisone (P16) (Fig. 2E, 3). Subsequent verification assays demonstrated that the selective physical removal of P4, P5, P9, and P10 significantly attenuated the overall antioxidant activity of the extract, strongly implying their synergistic nutritional efficacy within the food matrix (Fig. 2F). Conversely, P16 demonstrated a potential antagonistic effect, which corroborated the statistical predictions from the spectrum-effect relationship model. Finally, rather than simply identifying traditional quality markers, we intersected these validated knock-out compounds with the critical therapeutic targets predicted via network pharmacology to pinpoint the precise molecular effectors (Fig. 2G). This integrated multi-omics approach successfully prioritized four core dietary bioactive compounds and their corresponding interaction networks: rosmarinic acid (targeting PRSS1, CASP3, PTGS2, DPP4, PPARG, CDKN1A, STAT1, ESR1, and MAPK1), carnosic acid (PPARG, CYP19A1, and BCL2), carnosol (ACHE), and cirsimaritin (NCOA1, PTGS1, DPP4, NOS2, HSP90AA1, and NCOA2) (Fig. 2H).

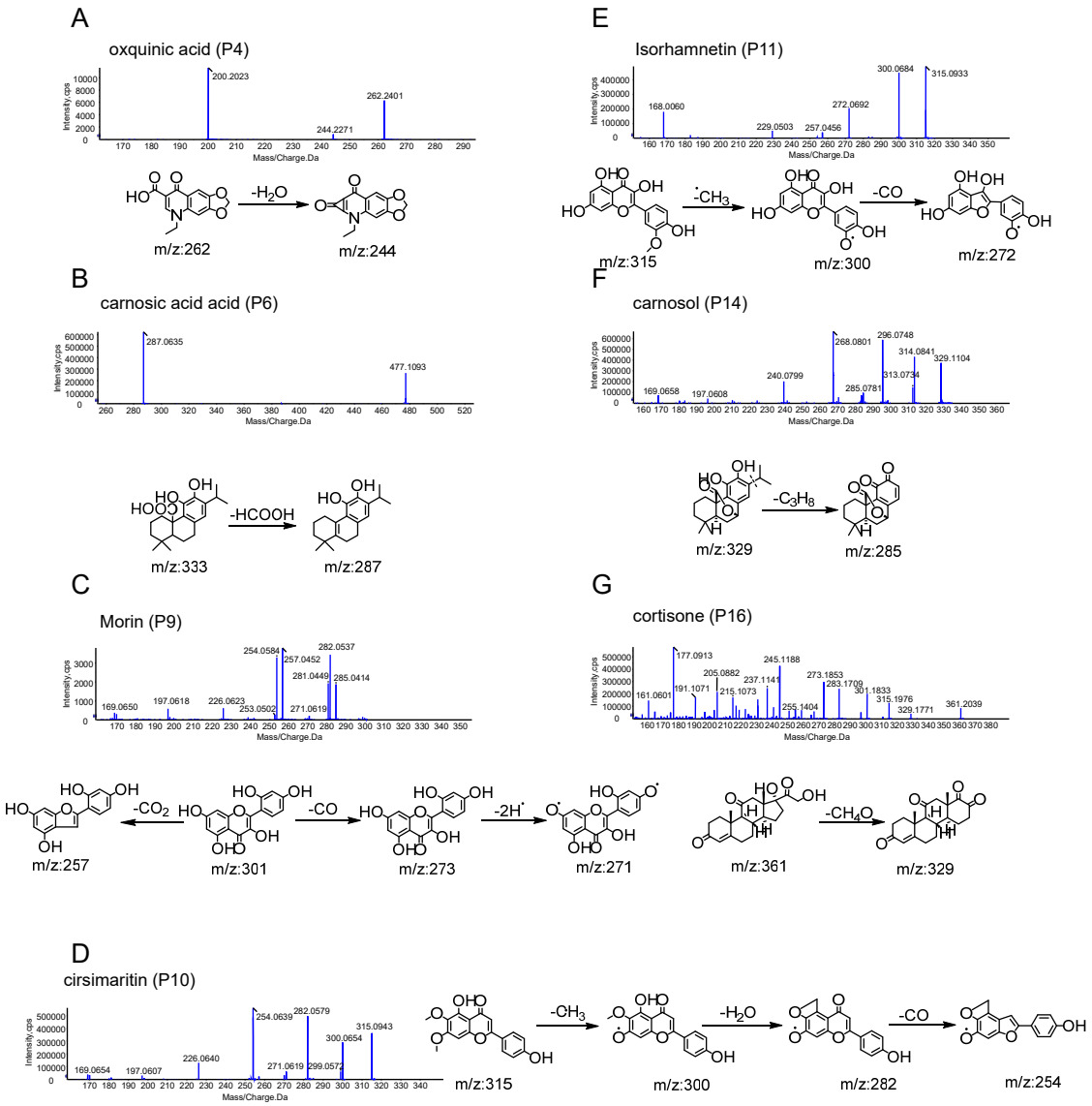

Fig. 3. Chemical structure of components extracted from Rosmarinus officinalis L.. The MS/MS fragmentation pathway and the MS/MS spectrum of (A) Oxquinic acid, (B) Carnosic acid, (C) Morin, (D) Cirsimaritin, (E) Isorhamnetin, (F) Carnosol, (G) Cortisone.

3.3 Evaluation of antioxidant efficacy and selection of the lead compound in HepG2 cells

To determine the safe dosage range, the cytotoxicity of the four candidate compounds (rosmarinic acid, carnosic acid, carnosol, and cirsimaritin) was first assessed using the MTT assay. As shown in Fig. 4A-D, none of the compounds exhibited significant cytotoxicity at concentrations up to 12.5 μM. Consequently, concentrations of 3.125, 6.25, and 12.5 μM were selected for subsequent bioactivity assays. Intracellular ROS levels were quantified to screen for the most potent antioxidant. Compared with the H_2O_2-induced model group, treatment with rosmarinic acid (RA), carnosic acid, and cirsimaritin significantly dose-dependently downregulated ROS generation ($P < 0.001$) (Fig. 4E-H). However, carnosol failed to show significant ROS scavenging activity in this cellular model. Further evaluation of oxidative stress markers (CAT, GSH, SOD, and MDA) confirmed the protective effects of the effective candidates. Consistent with the ROS results, RA, carnosic acid, and cirsimaritin effectively reversed H_2O_2-induced oxidative damage by restoring the activities of antioxidant enzymes (CAT, GSH, SOD) and reducing lipid peroxidation (MDA) (Fig. 4I-T). Notably, RA exhibited the superior antioxidant capacity among the candidates. Particularly at the highest tested concentration of 12.5 μM, RA treatment resulted in the most pronounced reduction in MDA content and excellent enzymatic recovery compared to the other groups. Based on these comprehensive in vitro findings, RA was designated as the lead compound for subsequent mechanistic studies.

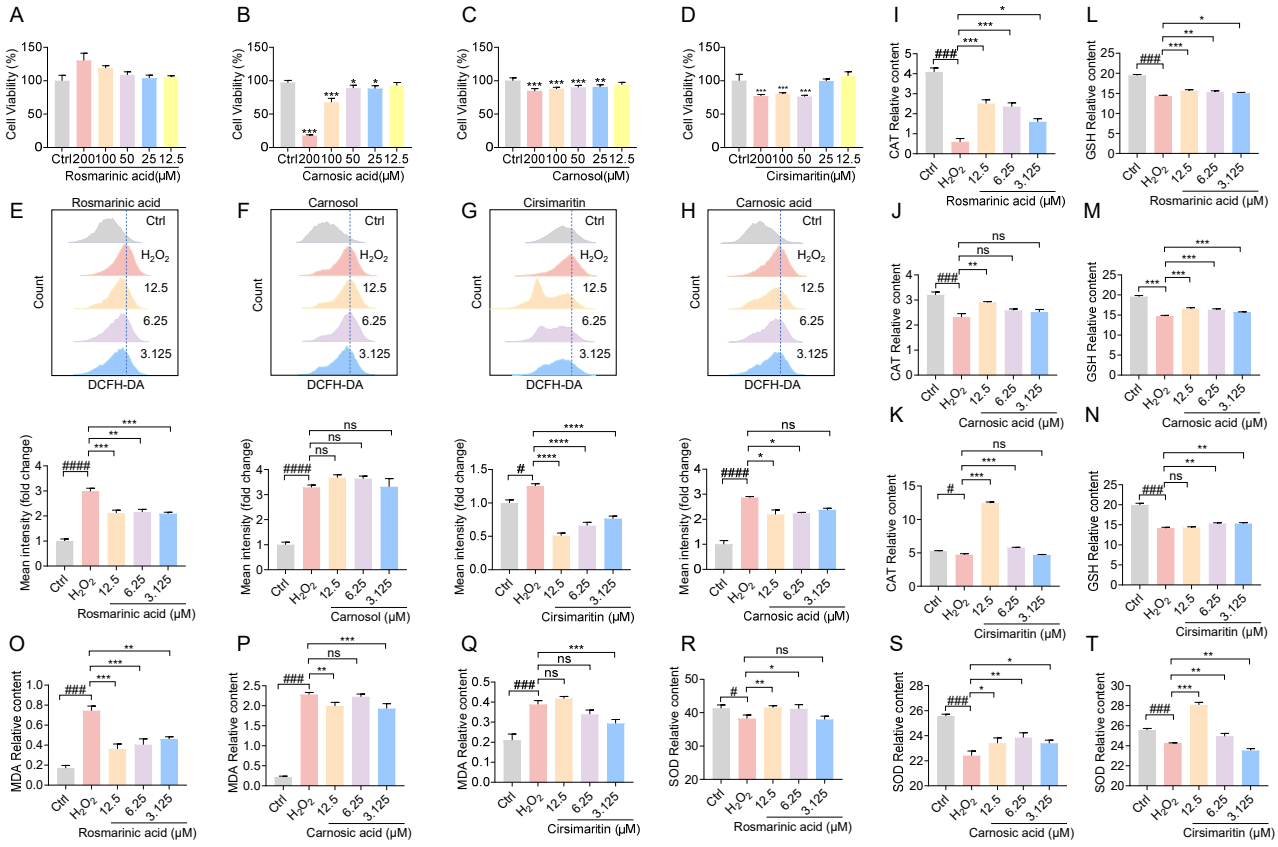

Fig. 4. Evaluation of antioxidant efficacy of candidate compounds in H_2O_2-induced HepG2 cells. (A-D) Cytotoxicity of Rosmarinic acid (RA), Carnosic acid, Carnosol, and Cirsimaritin on HepG2 cells determined by MTT assay. (E-H) Intracellular ROS levels detected by DCFH-DA staining and flow cytometry. (I-K) Effects of candidates on CAT activity. (L-N) Effects on GSH levels. (O-Q) Effects on MDA activity. (R-T) Effects on SOD content.

3.4 In vivo protective effects of RA against AAPH-induced oxidative stress in zebrafish

To validate the antioxidant efficacy of RA in vivo, an AAPH-induced zebrafish model was established following the experimental protocol depicted in Fig. 5A. Phenotypic analysis revealed that AAPH exposure triggered severe oxidative stress, characterized by significantly elevated ROS fluorescence and increased cell death compared to the control group. Notably, intervention with Vitamin C (positive control) and RA (at low, medium, and high doses) effectively mitigated these pathological changes, showing a significant reduction in both ROS accumulation (Fig. 5B) and cell mortality (Fig. 5C). At the transcriptional level, the impact of RA on the endogenous antioxidant defense system was evaluated. Compared with the model group, RA treatment significantly upregulated the mRNA expression levels of superoxide dismutase (sod), catalase (cat), and glutathione peroxidase (gpx) ($P < 0.05$) (Fig. 5D-F). These results confirm that RA exerts its protective effects in vivo by enhancing the expression of key antioxidant enzymes.

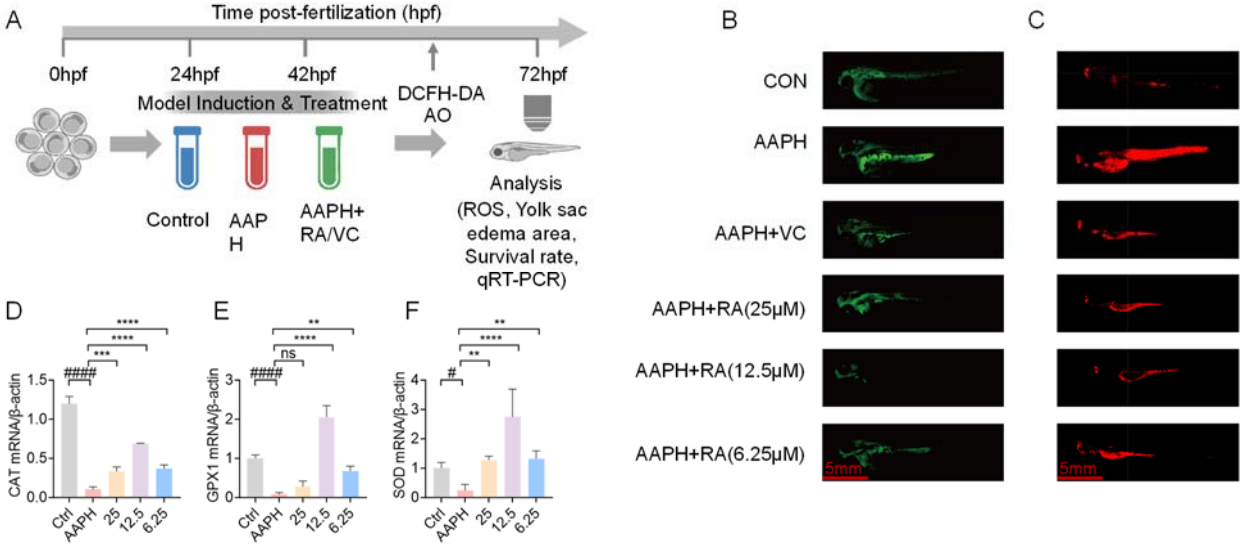

Fig. 5. In vivo protective effects of RA against AAPH-induced oxidative stress in zebrafish larvae. (A) Schematic diagram of the experimental protocol in zebrafish. (B) Representative fluorescence images of ROS generation. (C) Phenotypic observation of cell death in zebrafish larvae. (D-F) Relative mRNA expression levels of antioxidant enzymes (sod, cat, and gpx) determined by RT-qPCR.

3.5 Experimental validation of core targets at transcriptional and translational levels

To unravel the molecular mechanism, we examined the transcriptional response of predicted targets. Interestingly, the RT-qPCR results showed that H_2O_2 exposure led to a significant downregulation of *PPARγ*, *MAPK1*, *STAT1*, and *CASP3* mRNA levels compared to the control group (Fig. 6A-D), which might suggest a suppression of transcriptional machinery or specific pathway inhibition under severe oxidative stress. RA treatment significantly restored the expression of these genes, bringing them closer to the levels of the control group. However, mRNA levels do not always linearly correlate with protein function, especially for enzymes regulated by post-translational modification. Therefore, Western blot analysis was performed. As shown in Fig. 6E-H, at the protein level, RA effectively upregulated PPARγ. Crucially, despite the mRNA recovery, RA treatment significantly suppressed the phosphorylation of MAPK1 and STAT1, and inhibited the cleavage of Caspase-3. Furthermore, the mRNA expression of these core targets

was validated in vivo using the zebrafish model. As illustrated in Fig. 6I-L, compared with the model group, RA intervention significantly upregulated the expression of *pparg*, *mapk1*, *stat1*, and *casp3*. Collectively, these findings provide robust evidence that RA alleviates oxidative stress by modulating the PPARγ-mediated signaling pathway, involving the regulation of MAPK1, STAT1, and Caspase-3.

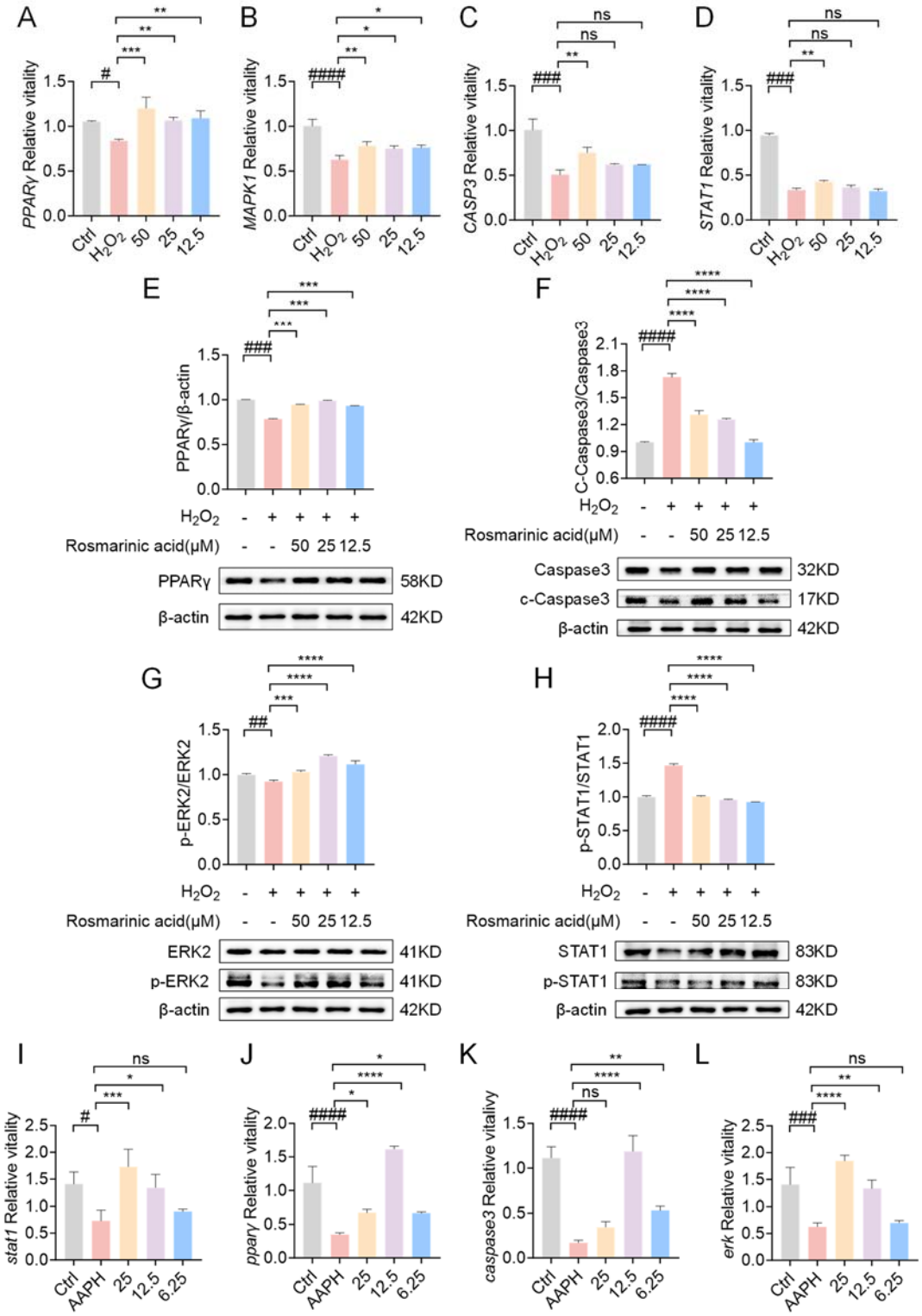

Fig. 6. Experimental validation of the core therapeutic targets at transcriptional and translational levels. (A-D) Relative mRNA expression of *PPARG*, *MAPK1*, *STAT1*, and *CASP3* in HepG2 cells treated with H_2O_2 and RA. (E-H) Representative Western blot bands and quantitative analysis of PPARγ, p-MAPK1/MAPK1, p-STAT1/STAT1, and Cleaved-Caspase-3/Caspase-3 in HepG2 cells. (I-L) Validation of mRNA expression levels (*pparg*, *mapk1*, *stat1*, and *casp3*) in the zebrafish model.

3.6 RA alleviates oxidative stress by binding to PPARγ and activating the Nrf2-NQO1 signaling axis

To elucidate the molecular interactions, molecular docking was performed to predict the binding affinity of RA with PPARγ, MAPK1, STAT1, and Caspase-3. As visualized in Fig. 7A-D, RA exhibited the strongest binding affinity to PPARγ (-9.038 kcal/mol) compared to other targets (Fig. 7E), forming stable hydrogen bonds with key residues such as SER-189 and LYS-367. To validate this direct interaction, CETSA was conducted. As shown in Fig. 7F, RA treatment remarkably enhanced the thermal stability of PPARγ protein in the temperature range of 49-69°C comparde to the DMSO control, confirming the direct target engagement between RA and PPARγ. Given that PPARγ activation can trigger the Nrf2 antioxidant pathway, we further investigated the downstream effectors. At the transcriptional level, RT-qPCR results indicated that the mRNA expression of *Nrf2* and *NQO1* was significantly suppressed in the model group. However, RA intervention effectively reversed this downregulation (Fig. 7G, H). Furthermore, Western blot analysis was employed to assess the protein levels of Total-Nrf2, Nuclear-Nrf2, and NQO1. As shown in Fig. 7I-K, oxidative stress compromised the antioxidant defense, evidenced by reduced levels of these proteins. Notably, RA treatment significantly upregulated the expression of Total-Nrf2 and NQO1. More importantly, RA markedly promoted the accumulation of Nuclear-Nrf2, suggesting that RA facilitates the nuclear translocation of Nrf2. Collectively, these findings demonstrate that RA specifically binds to PPARγ to promote Nrf2 nuclear translocation and NQO1 expression, thereby mitigating oxidative stress.

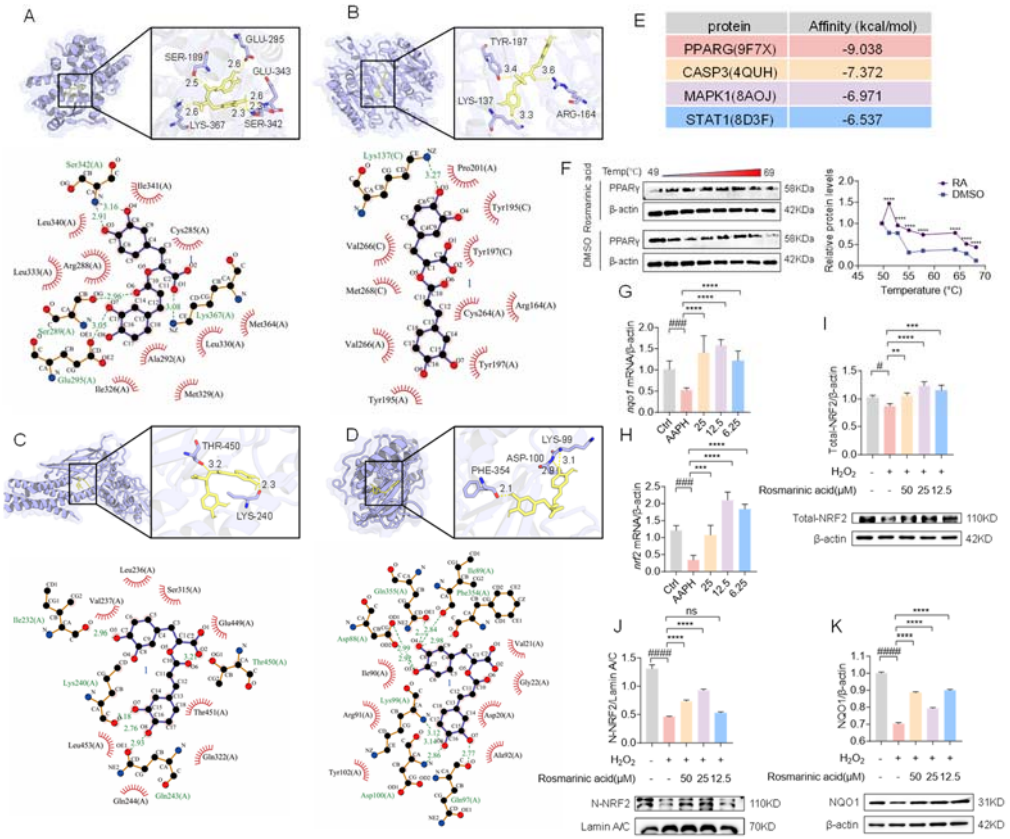

Fig. 7. Elucidation of the molecular mechanism: RA directly binds to PPARγ to activate the Nrf2 signaling axis. (A-D) Molecular docking simulations of RA with PPARγ, MAPK1, STAT1, and Caspase-3. (E) Comparison of binding energies. (F) Cellular Thermal Shift Assay (CETSA) confirming the direct physical binding and thermal stabilization of PPARγ by RA in living cells. (G-H) Relative mRNA expression of *nrf2* and *nqo1* in zebrafish. (I-K) Western blot analysis of Total-Nrf2, Nuclear-Nrf2, and NQO1 protein expression in HepG2 cells.

4. Discussion

Oxidative stress is widely recognized as a central driver in the pathogenesis of various chronic metabolic disorders, prompting an urgent demand for potent natural antioxidants suitable for dietary intervention[30, 31]. Despite the widespread consumption of rosemary as a prominent culinary herb and natural food preservative, the specific molecular link between its complex phytochemical profile and its health-promoting antioxidant properties remains poorly understood[32, 33]. Conventional bioassay-guided isolation methods are typically labor-intensive and often fail to capture the synergistic nutritional interactions present within complex food matrices[34]. To overcome these limitations, this research employed a multi-dimensional food-chemistry framework that merges untargeted metabolomics, network pharmacology, spectrum-effect modeling, and a novel "component knock-out" strategy. Unlike standard methodologies, our protocol extensively characterizes the dietary phytochemicals of rosemary via metabolomics before integrating these data with precision nutritional targets predicted by network pharmacology. This ensures that the identified bioactive candidates are stable and predominant constituents of the botanical matrix, irrespective of geographical variations. Furthermore, while prior computational analyses have broadly associated the antioxidant effects of rosemary to generic targets like TNF, CTNNB1, JUN, MTOR, and SIRT1 [35], the specific PPARγ-Nrf2/NQO1 axis elucidated in this study highlights a distinct dietary intervention pathway, underscoring the innovation of our integrated approach. Crucially, the "knock-out" method allowed for an accurate evaluation of the functional contributions of individual components within the intact food matrix. The successful establishment of this targeted component-deletion model and the subsequent identification of core dietary bioactive compounds offer a valuable methodological paradigm for investigating the nutritional material basis of other complex functional foods and dietary supplements.

Our integrated food-chemistry screening strategy highlighted rosmarinic acid (RA), carnosic acid, carnosol, and cirsimaritin as the primary dietary bioactive candidates. Among these, RA demonstrated a robust and potent antioxidant potency in the HepG2 cellular model. A notable divergence was observed regarding carnosol: while it exhibited robust radical scavenging potential in the chemical ABTS assay and showed a positive correlation in the spectrum-effect analysis, it failed to elicit a significant reduction in intracellular ROS levels. This discrepancy highlights a critical paradigm in nutritional research: intrinsic chemical redox capacity does not inevitably translate to physiological efficacy. This limitation is frequently attributable to restricted cellular uptake, poor membrane permeability, or extensive presystemic metabolism - common challenge in nutritional interventions[36]. Such findings emphasize the critical need to cross-validate chemical assays with biological models for a holistic assessment of dietary antioxidants. Consequently, by accurately quantifying the functional contribution of individual compounds within the intact dietary matrix, RA was designated as the principal functional compound, a status further corroborated by its robust protective activity in the *in vivo* zebrafish model, bridging the translational gap between chemical composition and *in vivo* efficacy.

A pivotal discovery of this investigation is the elucidation of the molecular mechanisms driving RA's health-promoting effects. The antioxidant activity and pleiotropic targets of RA have been previously documented; for instance, it mitigates toxin-induced oxidative tissue damage and cellular stress via diverse signaling cascades[37, 38]. While initial network pharmacology identified a broad array of potential targets, our experimental verification specifically focused on the PPARγ-Nrf2 axis. By employing CETSA-a robust biophysical assay for validating target engagement in physiological environments-we provided compelling empirical evidence that RA directly binds to the PPARγ protein and enhances its thermal stability. This experimental confirmation significantly provides a critical advantage over above studies relying exclusively on *in silico* docking predictions. Although PPARγ is classically characterized as a master regulator of lipid metabolism, accumulating evidence underscores its critical function in cellular redox homeostasis[39, 40]. Our data demonstrated that dietary RA intervention effectively restored PPARγ expression, which had been suppressed by oxidative stress. Furthermore, we confirmed that RA facilitates the nuclear translocation of Nrf2, subsequently upregulating the transcription of downstream antioxidant defense enzymes (NQO1, SOD, and CAT). Given that PPARγ acts as an upstream modulator of Nrf2, our findings strongly suggest that RA-activated PPARγ orchestrates a potent antioxidant response by transcriptionally regulating Nrf2. This identifies the "RA-PPARγ-Nrf2" signaling cascade as the primary molecular mechanism underlying its dietary efficacy.

Oxidative stress is intricately linked to cellular apoptosis and inflammatory responses[41]. Interestingly, our multi-level molecular analysis revealed a divergent transcriptional and post-translational response to the intervention. We found that severe H_2O_2-induced oxidative damage suppressed the mRNA expression of MAPK1, STAT1, and CASP3. However, RA treatment restored the expression of these genes to near-normal levels. This phenomenon likely reflects a global restoration of cellular transcriptional homeostasis following oxidative insult. Crucially, although mRNA levels recovered, our Western blot data confirmed that the functional protein levels exhibited a distinct, protective trend: RA treatment significantly reduced the phosphorylation of MAPK1 and STAT1, and effectively inhibited the activation of cleaved-Caspase-3. This uncoupling of mRNA and active protein expression provides profound mechanistic insight: the anti-apoptotic and anti-inflammatory efficacy of RA is primarily governed by modulating post-translational modifications (phosphorylation and cleavage cascades) rather than relying solely on transcriptional suppression. Related studies indicate that PPARγ acts upstream of STAT1 to inhibit its activity, thereby reducing inflammatory cascades[42]. Concurrently, the MAPK/ERK pathway is often triggered by ROS to propagate pro-apoptotic signals[43, 44]. By mapping these specific post-translational interventions, our study systematically explains how RA not only neutralizes the upstream oxidative inducers but also robustly blocks the downstream pathological consequences. This comprehensive mechanism elegantly explains the significant reduction in cellular apoptosis and ROS accumulation observed in our in vivo zebrafish model.

In summary, this study elucidates the dietary antioxidant material basis of rosemary by integrating spectrum-effect analysis with a novel component knock-out strategy. We definitively established RA as the primary functional ingredient. Mechanistically, RA operates not merely as a passive chemical scavenger but as a specific nutritional modulator that directly binds to PPARγ. This binding subsequently activates the Nrf2-NQO1 antioxidant pathway and suppresses MAPK/STAT/Caspase-3 apoptotic signaling to comprehensively mitigate oxidative stress (Fig. 8). These findings provide a novel, robust molecular foundation for the application of rosemary extracts and RA as high-value functional food ingredients and dietary supplements for health promotion.

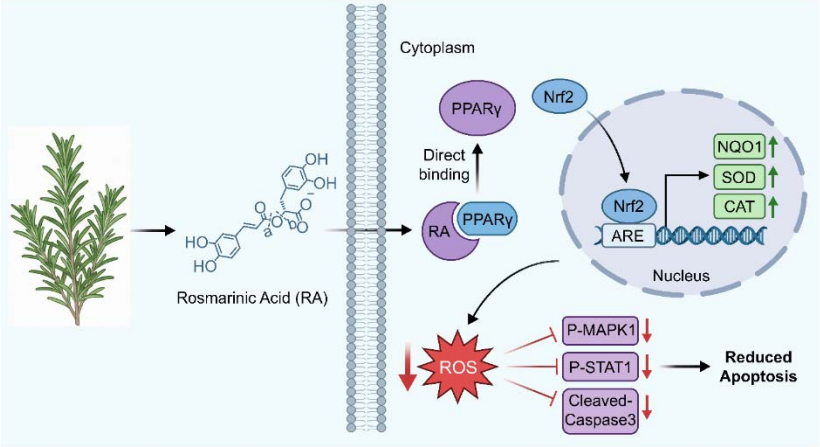

Fig. 8. Schematic representation of the proposed molecular mechanism of RA from *Rosmarinus officinalis* L..

5. Conclusion

In summary, this study successfully established a screening strategy combining metabolomics, spectrum-effect analysis, and a novel "component knock-out" method. Through this approach, we identified RA as the primary antioxidant Q-marker of rosemary. Our experiments in HepG2 cells and zebrafish confirmed that RA effectively reduces oxidative damage. Most importantly, we revealed the molecular mechanism: RA exerts its protective effect by directly binding to PPARγ and subsequently activating the Nrf2-NQO1 pathway. This work not only clarifies the material basis of rosemary but also provides a scientific basis for its potential use in treating oxidative stress-related diseases.

Declaration of competing interest

We declare that we have no financial or personal relationships with individuals or organizations that could inappropriately influence our work. There are no professional or personal interests in any product, service, or company that could be perceived as influencing the position presented in the manuscript or the review thereof.

Acknowledgments

This work was supported by the National Key Research and Development Program of China (2022YFF1100300) and Henan Provincial Major Science and Technology Special Project (231100310200).

Data availability

The data will be made available upon request.

Appendix A. Supplementary data

Supplemental information can be found online.

References

[1] Z. Liu, M. Wang, Y. Liu, et al., Patrinoside and Patrinoside A from Patrinia scabiosaefolia Improve Insulin Resistance by Inhibiting NF-κB, MAPK Pathways and Oxidative Stress in RAW264.7 and 3 T3-L1 Cells, Oxidative Medicine and Cellular Longevity. 2023 (2023) 9069645. https://doi.org/https://doi.org/10.1155/2023/9069645.

[2] F.M. El-Demerdash, Y. Talaat, R.A. El-Sayed, et al., Hepatoprotective Effect of Actinidia deliciosa against Streptozotocin-Induced Oxidative Stress, Apoptosis, and Inflammations in Rats, Oxidative Medicine and Cellular Longevity. 2022 (2022) 1499510. https://doi.org/https://doi.org/10.1155/2022/1499510.

[3] J.-B. Chen, G. Li, X. Chen, et al., Nutritional value and antioxidant activity of Artemisia princeps, an edible plant frequently used in folk food in the Xiangxi region, Food & Medicine Homology. 2 (2025) 9420043. https://doi.org/10.26599/FMH.2025.9420043.

[4] S. Govindan, A. Jayabal, J. Shanmugam, et al., Antioxidant and hepatoprotective effects of Hypsizygus ulmarius polysaccharide on alcoholic liver injury in rats, Food Science and Human Wellness. 10 (2021) 523-535. https://doi.org/https://doi.org/10.1016/j.fshw.2021.04.015.

[5] J.-K. Zhang, X.-L. Zhou, X.-Q. Wang, et al., Que Zui tea ameliorates hepatic lipid accumulation and oxidative stress in high fat diet induced nonalcoholic fatty liver disease, Food Research International. 156 (2022) 111196. https://doi.org/https://doi.org/10.1016/j.foodres.2022.111196.

[6] C. Duan, D. Jiao, H. Wang, et al., Activation of the PPARγ Prevents Ferroptosis-Induced Neuronal Loss in Response to Intracerebral Hemorrhage Through Synergistic Actions With the Nrf2, Frontiers in Pharmacology. Volume 13 - 2022 (2022) https://doi.org/10.3389/fphar.2022.869300.

[7] Y. Liu, F. Wang, H. Xu, et al., Ginkgolide B attenuates hyperlipidemia by restoring sphingolipid homeostasis and activating PPARα and Nrf2 pathways, Scientific Reports. 15 (2025) 28774. https://doi.org/10.1038/s41598-025-14626-4.

[8] G. Fu, Y. Yan, Y. Li, et al., Genistein-7-O-octanoate: a promising natural antioxidant for stabilizing soybean oil during storage and high-temperature frying, Food Research International. 226 (2026) 118257. https://doi.org/https://doi.org/10.1016/j.foodres.2025.118257.

[9] D.-X. Sun-Waterhouse, X.-Y. Chen, Z.-H. Liu, et al., Transformation from traditional medicine-food homology to modern food-medicine homology, Food & Medicine Homology. 1 (2024) 9420014. https://doi.org/10.26599/FMH.2024.9420014.

[10] X.-Y. Sun, X.-S. Xiang, Y.-J. Zhou, et al., Global policy changes on homologous substances of food and medicine, Food & Medicine Homology. 3 (2026) 9420126. https://doi.org/10.26599/FMH.2026.9420126.

[11] H. Bendif, M. Boudjeniba, M. Djamel Miara, et al., Rosmarinus eriocalyx: An alternative to Rosmarinus officinalis as a source of antioxidant compounds, Food Chemistry. 218 (2017) 78-88. https://doi.org/https://doi.org/10.1016/j.foodchem.2016.09.063.

[12] W. Yeddes, I. Bettaieb Rebey, H. Manai-Djebali, et al., Assessing the efficacy of rosemary extract as a natural preservative for enhancing oxidative stability and preventing rancidity in linseed oil, Journal of Food Measurement and Characterization. 19 (2025) 2252-2263. https://doi.org/10.1007/s11694-025-03107-x.

[13] B. Jia, J. Shang, H. Zeng, et al., Hepatoprotective Effects of Rosmarinic Acid on Ovalbumin-Induced Intestinal Food Allergy Mouse Model, Molecules. 28 (2023) 788. https://www.mdpi.com/1420-3049/28/2/788

[14] M. Ghasemzadeh Rahbardar, B. Amin, S. Mehri, et al., Anti-inflammatory effects of ethanolic extract of Rosmarinus officinalis L. and rosmarinic acid in a rat model of neuropathic pain, Biomedicine & Pharmacotherapy. 86 (2017) 441-449. https://doi.org/https://doi.org/10.1016/j.biopha.2016.12.049.

[15] S. Lešnik, V. Furlan, U. Bren, Rosemary (Rosmarinus officinalis L.): extraction techniques, analytical methods and health-promoting biological effects, Phytochemistry Reviews. 20 (2021) 1273-1328. https://doi.org/10.1007/s11101-021-09745-5.

[16] J. Moore, M. Yousef, E. Tsiani, Anticancer Effects of Rosemary (Rosmarinus officinalis L.) Extract and Rosemary Extract Polyphenols, Nutrients. 8 (2016) 731. https://www.mdpi.com/2072-6643/8/11/731

[17] W. Zhou, Y. Wang, A network-based analysis of the types of coronary artery disease from traditional Chinese medicine perspective: Potential for therapeutics and drug discovery, Journal of Ethnopharmacology. 151 (2014) 66-77. https://doi.org/https://doi.org/10.1016/j.jep.2013.11.007.

[18] D. Jiang, J. Xu, S. Liu, et al., Rosmanol induces breast cancer cells apoptosis by regulating PI3K/AKT and STAT3/JAK2 signaling pathways, Oncol Lett. 22 (2021) 631. https://doi.org/10.3892/ol.2021.12892.

[19] J. Eberhardt, D. Santos-Martins, A.F. Tillack, et al., AutoDock Vina 1.2.0: New Docking Methods, Expanded Force Field, and Python Bindings, Journal of Chemical Information and Modeling. 61 (2021) 3891-3898. https://doi.org/10.1021/acs.jcim.1c00203.

[20] O. Trott, A.J. Olson, AutoDock Vina: Improving the speed and accuracy of docking with a new scoring function, efficient optimization, and multithreading, Journal of Computational Chemistry. 31 (2010) 455-461. https://doi.org/https://doi.org/10.1002/jcc.21334.

[21] S.L. Matić, N. Tomašević, M. Božović, et al., Hesperetin's antigenotoxicity: the impact on EMS-made lesions within Drosophila melanogaster somatic cells' DNA, disclosed through molecular modeling, Phytomedicine. 150 (2026) 157728. https://doi.org/https://doi.org/10.1016/j.phymed.2025.157728.

[22] H. Zhang, Q. Guo, Z. Liang, et al., Anti-inflammatory and antioxidant effects of Chaetoglobosin Vb in LPS-induced RAW264.7 cells: Achieved via the MAPK and NF-κB signaling pathways, Food and Chemical Toxicology. 147 (2021) 111915. https://doi.org/https://doi.org/10.1016/j.fct.2020.111915.

[23] Q. Wang, S. Wang, L. Cui, et al., Flammulina velutipes polysaccharide exerts immunomodulatory function involving RSAD2 to regulate the NF-κB/MAPK signaling pathway in RAW264.7 macrophage cells and in mouse spleen cells, International Journal of Biological Macromolecules. 309 (2025) 142985. https://doi.org/https://doi.org/10.1016/j.ijbiomac.2025.142985.

[24] Y. Zheng, Y. Yu, J. Feng, et al., Unveiling the Potential of Nelumbo nucifera-Derived Liensinine to Target The Myostatin Protein and to Counteract Muscle Atrophy, Journal of Agricultural and Food Chemistry. 72 (2024) 2240-2249. https://doi.org/10.1021/acs.jafc.3c09002.

[25] L.-L. Gao, X.-T. Fang, S.-H. Zhao, et al., Naphthoquinone Derivatives from the Endophytic Fungus Fusarium solani Induce Pancreatic Cancer Cells Apoptosis via Targeting EGFR-Mediated PI3K/Akt Pathway, Journal of Agricultural and Food Chemistry. 72 (2024) 26209-26223. https://doi.org/10.1021/acs.jafc.4c08652.

[26]X. Liu, X. Meng, D. Liu, et al., A rapid analysis method to discover antioxidant active components and mechanisms in soybean: untargeted metabolomics combined with network pharmacology and spectrum-effect relationship-component knockout-identification techniques, Food Science and Human Wellness. 14 (2025) 9250620. https://doi.org/10.26599/FSHW.2025.9250620.

[27] Z. Liang, Q. Tang, H. Liang, et al., Glucomannogalactan inhibits senescence by promoting nuclear translocation of NRF2, Int J Biol Macromol. 305 (2025) 141059. https://doi.org/10.1016/j.ijbiomac.2025.141059.

[28] Q. Tang, Z.-H. Liang, J.-J. Yuan, et al., FER1L6 ameliorates insulin resistance by regulating GLUT4 expression, Food & Medicine Homology. 2 (2025) 9420070. https://doi.org/10.26599/FMH.2025.9420070.

[29] Z.-H. Liu, B.-B. Yu, H.-H. Zhou, et al., Characteristic components from Rehmannia radix and their effects on insulin resistance through PI-3K/AKT signaling pathway in HepG2 Cells, Food & Medicine Homology. 2 (2025) 9420073. https://doi.org/10.26599/FMH.2025.9420073.

[30] H. Rajan, B.-H. Goh, Y. Kumari, et al., Potential of Cyclodipeptides in Combating Oxidative Stress in Chronic Diseases, Pharmacological Research. (2025) 108076. https://doi.org/https://doi.org/10.1016/j.phrs.2025.108076.

[31] D. Weismann, K. Hartvigsen, N. Lauer, et al., Complement factor H binds malondialdehyde epitopes and protects from oxidative stress, Nature. 478 (2011) 76-81. https://doi.org/10.1038/nature10449.

[32] R. Upadhyay, H.N. Mishra, Antioxidant activity measurement of oleoresin from rosemary and sage, Industrial Crops and Products. 61 (2014) 453-459. https://doi.org/https://doi.org/10.1016/j.indcrop.2014.07.043.

[33] H.-Y. Liang, M. Guan, T.-H. Li, et al., Critical review on biological effect and mechanisms of diterpenoids in Rosmarinus officinalis, Food & Medicine Homology. 2 (2025) 9420021. https://doi.org/10.26599/FMH.2025.9420021.

[34] C. Hernández-Hernández, V.M. Fernández-Cabanás, G. Rodríguez-Gutiérrez, et al., Viability of near infrared spectroscopy for a rapid analysis of the bioactive compounds in intact cocoa bean husk, Food Control. 120 (2021) 107526. https://doi.org/https://doi.org/10.1016/j.foodcont.2020.107526.

[35] A. Bisht, D. Tewari, S. Kumar, et al., Network pharmacology-based approach to investigate the molecular targets and molecular mechanisms of Rosmarinus officinalis L. for treating aging-related disorders, Biogerontology. 25 (2024) 793-808. https://doi.org/10.1007/s10522-024-10122-w.

[36] N. Hidalgo-Liberona, R. González-Domínguez, E. Vegas, et al., Increased Intestinal Permeability in Older Subjects Impacts the Beneficial Effects of Dietary Polyphenols by Modulating Their Bioavailability, Journal of Agricultural and Food Chemistry. 68 (2020) 12476-12484. https://doi.org/10.1021/acs.jafc.0c04976.

[37] Y. Yu, Y. Wu, H.-z. Yan, et al., Rosmarinic acid ameliorates acetaminophen-induced acute liver injury in mice via RACK1/TNF-α mediated antioxidant effect, Pharmaceutical Biology. 59 (2021) 1284-1291. https://doi.org/10.1080/13880209.2021.1974059.

[38] H. Rong, Y. Liang, Y. Niu, Rosmarinic acid attenuates β-amyloid-induced oxidative stress via Akt/GSK-3β/Fyn-mediated Nrf2 activation in PC12 cells, Free Radical Biology and Medicine. 120 (2018) 114-123. https://doi.org/https://doi.org/10.1016/j.freeradbiomed.2018.03.028.

[39] S.H. Attia, S.M. Elshazly, M.M. Abdelaal, et al., Reno-protective effect of mangiferin against methotrexate-induced kidney damage in male rats: PPARγ-mediated antioxidant activity, Saudi Pharmaceutical Journal. 30 (2022) 1252-1261. https://doi.org/https://doi.org/10.1016/j.jsps.2022.06.026.

[40] K. Kim, K. Boo, Y.S. Yu, et al., RORα controls hepatic lipid homeostasis via negative regulation of PPARγ transcriptional network, Nature Communications. 8 (2017) 162. https://doi.org/10.1038/s41467-017-00215-1.

[41] D. Coimbra-Costa, N. Alva, M. Duran, et al., Oxidative stress and apoptosis after acute respiratory hypoxia and reoxygenation in rat brain, Redox Biology. 12 (2017) 216-225. https://doi.org/https://doi.org/10.1016/j.redox.2017.02.014.

[42] B. Bajgai, M. Suri, H. Singh, et al., Naringin: A flavanone with a multifaceted target against sepsis-associated organ injuries, Phytomedicine. 130 (2024) 155707. https://doi.org/https://doi.org/10.1016/j.phymed.2024.155707.

[43] Y. Xie, D. Fan, B. Wu, et al., PM2.5 promotes platelet activation and thrombosis via ROS/MAPKs pathway-mediated mitochondrial dysfunction, Environmental Research. 283 (2025) 122116. https://doi.org/https://doi.org/10.1016/j.envres.2025.122116.

[44] J. Wang, L. Guo, X. Hao, et al., Nontargeted metabolomics combining with intestinal microbiota and hypolipidemia targets elucidates anti-hyperlipidemia effect of Sangju yinzha tea in hyperlipidemia rats, Food Bioscience. 65 (2025) 106012. https://doi.org/https://doi.org/10.1016/j.fbio.2025.106012.